KSCE Journal of Civil Engineering (2021) 25(1):70-77
DOI 10.1007/s12205-020-0497-0

pISSN 1226-7988, eISSN 1976-3808
www.springer.com/12205

Geotechnical Engineering

Mechanical Properties and Microstructure of Lime-Treated Red Clay

Lijie Chen[a], **Xuejun Chen**[a], **He Wang**[b], **Xiang Huang**[a], **and Yu Song**[a]

[a]*College of Civil and Architecture Engineering, Guilin University of Technology, Guilin 541004, China*
[b]*State Key Laboratory for Disaster Prevention & Mitigation of Explosion & Impact, Army Engineering University, Nanjing 210007, China*

ARTICLE HISTORY

Received 19 March 2020
Revised 5 July 2020
Accepted 11 August 2020
Published Online 4 November 2020

KEYWORDS

Lime
Red clay
Microstructure
Mechanics
Calcium oxide

ABSTRACT

This research conducted a triaxial test on lime-treated clay with different contents to analyze the effect of mechanical properties. Scanning electron microscope (SEM) and low-field nuclear magnetic resonance (NMR) analysis were used to analyze the effect. X-ray diffraction (XRD) was used to analyze the chemical changes of calcium oxide on red clay. The results show that with the increase of calcium oxide content, the strength increases, and it can be increased by 282% at 200 kPa confining pressure. The calcium oxide in the red clay reacted with the water in the soil to form calcium hydroxide. The alkaline environment will erode the edge of the soil particles and cause pores to become larger. SEM observed that the addition of calcium oxide caused the agglomeration of soil particles and changed the pore structure of red clay. Low-field NMR showed that calcium oxide had a significant effect on the pore structure of red clay. Calcium oxide increased the total pore volume of the soil sample. Calcium oxide had a substantial influence on the three pore distribution ranges, I (1.1 – 11 μm), II (15 – 137 μm), and III (137 – 512 μm). The porosity fitted with shear strength, it negatively correlated with I and III, and positively correlated with II.

1. Introduction

Since K. Terzaghi proposed the concept of soil structure in 1925, many researcher have conducted further research and found that the microstructure of soil is an essential factor affecting engineering characteristics such as strength and permeability. The macroscopic and microscopic structure of the soil changed significantly, the evolution of pore distribution predicted the change (Tchalenko and Morgenstern, 1967; Tovey, 1980; Delage and Lefebvre, 1984; Al-Mukhtar et al., 1996; Koliji et al., 2010; Oualmakran et al., 2016; Shan et al., 2016; Lv et al., 2018). Alonso et al. (2013) measured and quantitatively analyzed the pore microstructure of dry and wet compacted soil by mercury intrusion porosimetry (MIP). Lin and Cerato (2015) used scanning electron microscopy (SEM) to observe the microscopic characteristics of expansive soils and explained their micromechanical behavior through microscopic traits. Most of these studies used MIP and SEM to analyze the pore structure characteristics of the soil. However, the main problem of the application is that the MIP test tube is small in size and can only take a part of the soil sample for testing, which is difficult to reflect the overall pore distribution of the sample. Besides, mercury is toxic, and invasive mercury samples can pollute the environment, so it is essential to measure soil pores using more environmentally friendly and reliable testing methods.

Because low-field NMR is sensitive to hydrogen-containing fluids, it has used to analyze the distribution and transmission of water in porous media. Fleury et al. (2019) investigated the diffusion of water in industrial cement and concrete using low-field NMR. Liang et al. (2019) combined the amott wettability test with low-field NMR to characterize the wettability of dense sand. Low-field NMR is non-destructive and sensitivity to fluid distribution for the distribution of water, it can be used to evaluate wettability (Wang et al., 2019). Low-field NMR reflected the microstructure of rocky and soil, and it used to analyze the microscopic soil structure (Gallegos and Smith, 1988; Jaeger et al., 2009; Daigle and Johnson, 2016).

Red clay is a peculiar soil with high porosity, high water content, high liquid-plastic limit. It will soften when the water content increases (Ghobadi et al., 2014). If it is not treated in the project, it may cause problems such as slope instability, reservoir leakage, etc., or the sub-grade collapse due to an inadequate

CORRESPONDENCE Xuejun Chen xuejunchen@126.com College of Civil and Architecture Engineering, Guilin University of Technology, Guilin 541004, China

foundation bearing capacity. In engineering, red clay usually replaced by soil with better engineering properties, but the replaced red clay needs to be stacked separately, and excessively high red clay may cause landslides and damage the environment (Kilic et al., 2016). Some researchers have stabilized the soil by calcium carbonate, glass fiber, and other materials (Changizi and Haddad, 2017; Chen et al., 2020). Using lime to treat cohesive soil is typical behavior in engineering (Zhao et al., 2014; Yunus et al., 2016; Eltwati et al., 2020). Many researcher have done a lot of studies on lime stabilized soil and found that adding lime can enhance its mechanical properties. The optimal lime content was about 7% (Sakr et al., 2008; Kilic et al., 2016; Zimmermann et al., 2019). When lime mixed with the clay, its plasticity limit will decrease (Bell, 1996). Lime and soil also undergo ion exchange, flocculation, and agglomeration. And lime itself has a specific carbonization effect. The chemical reactions caused significant changes in the structure of lime-stabilized soil (Guidobaldi et al., 2018). At the same time, lime is considered to be a stabilizer for soil pollution, which can effectively reduce the reduced leaching capacity (Saeed et al., 2015).

Many researchers had studied the microstructure of lime-stabilized clay by experiments such as SEM and MIP (Lemaire et al., 2013; Saba et al., 2014; Bozbey, 2018). There are few studies on the analysis of the micropore structure of lime-treated clay based on low-field NMR. With the advantage of low-field NMR, there is no limit to the pore size measurement range, a complete sample that can be measurable.

This research mainly studied the effect of calcium oxide content on the strength of red clay, used the sensitivity of low-field NMR hydrogen atoms to test the pore distribution of calcium oxide on saturated samples, observe the microstructure with SEM, analyze the chemical influence of calcium oxide on red clay by XRD.

Table 1. The Physical and Mechanical Property of Red Clay

Natural moisture content (%)	27.2
The relative density of soil particles (g/cm^3)	2.7
Liquid limit (%)	61
Plastic limit (%)	45
Maximum dry density (g/cm^3)	1.55
Optimal moisture content (%)	30

Table 2. Composition of Calcium Oxide

Ingredient	Content/%
CaO	≥ 98
Acetic acid insoluble matter	0.1
Burning vector	2
Chloride (Cl)	0
Sulfate (SO_4)	0.1
Iron (Fe)	0
Heavy metals (as Pb)	0
Alkali metals and magnesium	0.5

2. Materials

The red clay used in the test was from a depth of 5 m in Yanshan, Guilin, China. Its fundamental physical and mechanical parameters are shown in Table 1. The chemical components of the calcium oxide are shown in Table 2. The calcium oxide does not contain heavy metals such as chloride, iron, and lead.

3. Mechanical Testing

3.1 Red Clay Preparations

Screened the air-dried red clay with a particle size of less than 2 mm, and then mixed the calcium oxide powder into the air-dried red clay at mass ratios of 0%, 1%, 2%, and 8%. Mixed the air-dried red clay particles with calcium oxide powder uniformly and spray into a certain amount of pure water to make the water content 30% (optimal water content), seal for 24 h to make the water uniform in the soil, and retest the water content (30% 0.5%).

3.2 Triaxial Compression Shear Tests

The sample with height, diameter, and dry density were 80 mm, 39.1 mm, 1.40 g/cm^3, respectively. The clay is difficult to saturate, and we saturate the sample according to the vacuum saturation method in the Chinese Standard for Soil Test Method (GB/T 50123-1999, 1999) to increase the saturation of the sample and shorten the time. Fix the sample with a saturer, put it into a metal bucket, and vacuum for 2 h (at a pressure -0.101 MPa). Inject pure water while maintaining the negative pressure, and open the air valve after the sample is immersed in the water, and keep it immersed in the water for 24 h. We have tested some samples with different dry densities (1.4, 1.5, 1.6 g/cm^3) saturated by the vacuum saturation method, and the levels are all above 98%. The unconsolidated-undrained triaxial tests (ASTM D2850-15, 2013) performed with a TKA-TTS-1 triaxial instrument of Nanjing TKA Technology Co., Ltd, and the compress at a rate of 0.8 mm/min. When the stress peaked, or the axial strain at 15%, the test stopped. If there is no peak, take the stress corresponding to 15% of the strain as the peak.

3.3 Low-Field NMR Tests

NMR refers to the response of the atomic nucleus to the magnetic field. For most atomic nuclei in the formation, the NMR signal caused by the external magnetic field is tiny, which can not be detected by an NMR instrument and does not disturb the test signal. The hydrogen nucleus is rich in water, it has only one proton without neutrons, has a massive magnetic moment and generates a strong signal, which is easily detected by the NMR instrument. The low-field NMR used to study rock and soil based on the response of hydrogen nuclei. When an external magnetic field is present, the hydrogen nucleus precesses around the direction of the external magnetic field. The spin hydrogen nucleus interacts with the external magnetic field to generate a measurable signal. The spin hydrogen atom polarized by

absorbing radio frequency in a static magnetic field. When the radio frequency terminated, the pulses absorbed by the polarized atoms are released. With a specific pulse sequence, the magnetization vector decay signal can be detected. The signal size is proportional to the number of hydrogen nuclei, and the decay time of the transverse magnetization vector is T_2. Generally, the lateral relaxation time of water in pores with different pore sizes is different. The distribution of T_2 relaxation time can reflect the pore structure. The shorter the relaxation time, the smaller the pore size.

We used a polytetrafluoroethylene (PTFE)mold that did not interfere with the NMR signal. The soil with a moisture content of 30% pressed into a circular PTFE mold with a height of 20 mm and an inner diameter of 60 mm, the dry density of the soil sample was 1.40 g/cm^3. The sample was evacuated and then soaked with pure water 24 h for NMR testing.

The NMR tests use the MacroMR12 micropore structure analysis and imaging system of Suzhou Niumag Analytical Instrument Co., Ltd. The magnetic field strength of the measured magnet unit was 0.3 Tesla. The polarization time (TW) is 1,000 ms, and the echo interval (TE) is 0.5 ms. The number of repetitions (NS) is 16 times, and the pulse (NECH) is 1,000. After the tests, the inverse performed by simultaneous iterative reconstruction technology (SIRT) and 10,000 iterative fittings performed to obtain a T_2 spectrum test signal.

4. Results and Discussion

4.1 Triaxial Compression Test

According to the calcium oxide contain and cohesion in Fig. 1, the cohesion and compression strength positively correlated with calcium oxide content. The calcium oxide content is less than 2%, and the cohesion increases significantly as the calcium oxide content increases. The calcium oxide content exceeds 4%; the cohesion growth slows down. The calcium oxide content is less than 2%, the hydration reaction completed, and the cohesion significantly increases. Because the calcium oxide content increases, leading to cumulative hydration products gradually increase, so the cohesion increases. The aluminosilicate produced by the volcanic ash reaction plays a cementing role (Saba et al., 2014). The cementation between particles is one of the main factors affecting soil cohesion, which makes the soil cohesion increase with the addition of calcium oxide.

It can be seen from Fig. 2 that the stress-strain relationship under 200 kPa confining pressure. The stress of the samples with 0% and 1% calcium oxide content increases with axial strain, and there is no peak. Shows that its stress-strain curve has strain-hardening characteristics. However, when the calcium oxide content exceeds 2%, the stress will decrease rapidly once a maximum appears, and the curve shows softening characteristics. The strength comes from the cohesion of the cement between particles and the friction between soil particles. As the calcium oxide content increases, the content of hydrated cement increases, leading the cohesion to increase. Therefore, the strength of the sample increases with the calcium oxide content. The cohesion generated by the cement can make the sample reach the maximum at a small axial strain. Because cement is brittle, once it exceeds the strength it can bear, it will break and cause the cohesion of the soil sample to disappear, so the strength drops rapidly when it reaches the peak. Therefore, with more calcium oxide, the stress-strain curve of the sample shows brittleness. When the calcium oxide content is less than 1%, the cement content is small. The internal friction angle mainly provides the strength of the sample. When the calcium oxide content is low, the content of the hydration product is also tiny. When the soil sample is compressed, the brittle fracture of the cement will not cause the sample stress curve to drop suddenly. Therefore, the stress-strain curve of the red clay treated with 1% calcium oxide still shows hardening characteristics.

According to the peak stress curve of stress in Fig. 3, calcium oxide effectively increases the strength of red clay. When the calcium oxide content is 1%, the strength changes little. When the calcium oxide content is higher than 1%, the peak of the

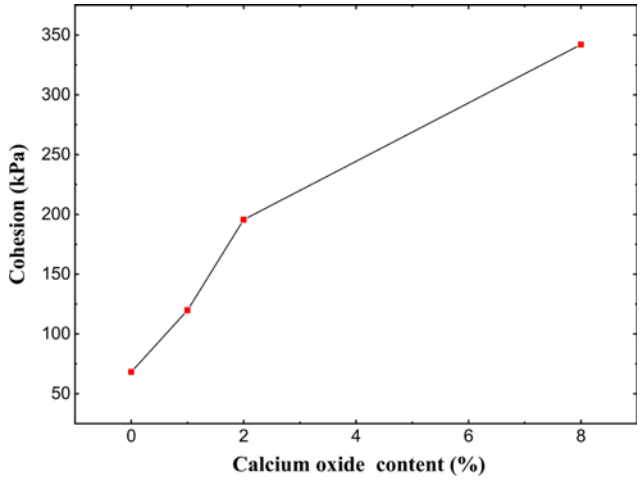

Fig. 1. Calcium Oxide Content and Cohesion

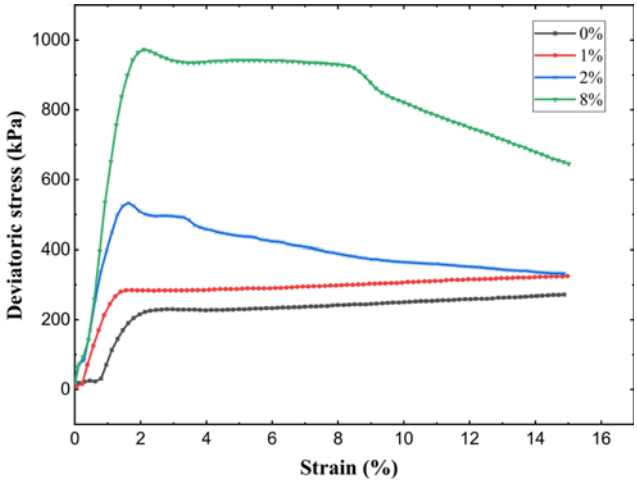

Fig. 2. Stress-Strain Curve under 200 kPa Confining Triaxial Unconsolidated and Undrained Shear

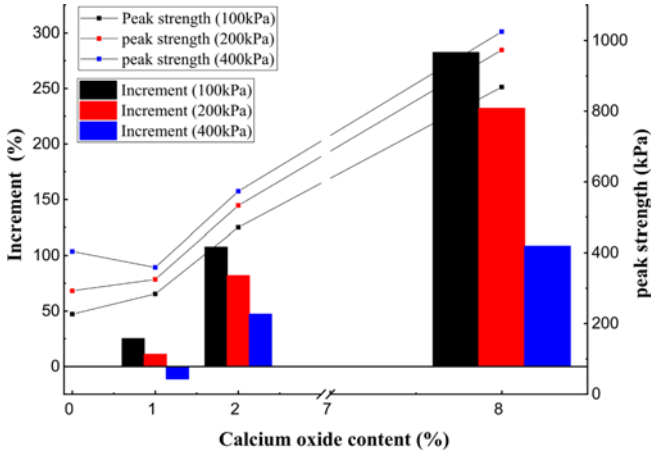

Fig. 3. The Peak Value of Eccentric Stress and Increment in the Strength of Lime-Treated Red Clay

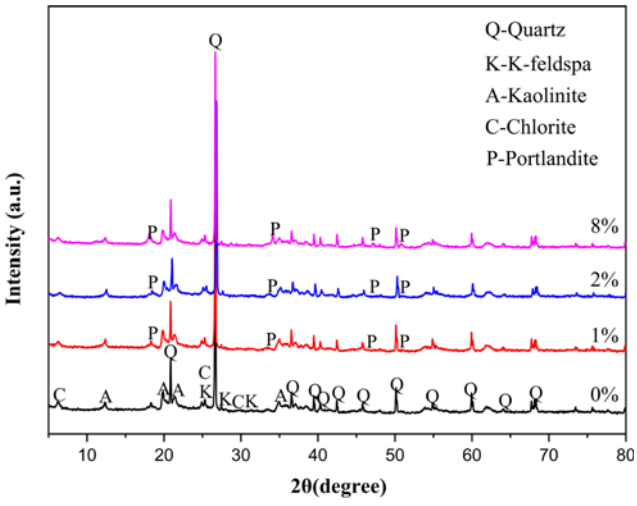

Fig. 4. XRD Spectrum of Lime-Treated Red Clay

stress increases significantly. The 8% calcium oxide content has the best effect on strength enhancement. With the same calcium oxide content, the larger the confining pressure, the smaller increase in the deviatoric stress. At a confining pressure of 200 kPa, the strength of 8% lime-treated red clay increased by 282%.

4.2 XRD Analysis

According to the XRD spectrum of Fig. 4, the mineral of red clay is quartz, potassium feldspar, kaolin, and chlorite. For the samples with Calcium oxide, new reflections can be seen. The d-spacings are 2.62, 4.90, 1.92, 1.79, 3.10, 1.68, 1.48, and 1.45. It is a characteristic peak of calcium hydroxide, which is due to oxidation calcium and water to form calcium hydroxide. However, Calcium oxide was not found in the samples (1%, 2%, and 8%), indicating that the Calcium oxide in the red clay completely reacted with the water. Bell (1996) and Ghobadi (2014) found that lime and kaolin reaction produce CSH, $C_3S_2H_3$ (calcium silicate hydrates), C_4AH_{13}, CAH_{10}, and $CaAH_{11}$ (calcium aluminate hydrates), due to the carbonization of lime will also generate $CaCO_3$. Still, the above products have not found by X-ray diffraction. Because the curing time did not consider, the sample only saturated in water for 24 h, and the hydration reaction time is short, so the amount of product produced is tiny and cannot be detected.

4.3 SEM Analysis

Compared with Figs. 5(a) and 5(b), a small amount of calcium oxide has little effect on the microstructure. From the stress-strain curve of 1% calcium oxide content in Fig. 1 that a small mass of calcium oxide has little effect on the plasticity. However, with 8% calcium oxide content (Fig. 5(c)), the particle morphology changed significantly, the particle aggregation. The structure of red clay turning from the granular and lamellar structure to the aggregate structure. The stress-strain curve of 8% calcium oxide content in Fig. 1 becomes softened, indicated that the content of calcium oxide affects the structure and changes the stress-strain curve. The aggregation of soil particles makes it have a visible skeleton structure, which leads to the shear strength and cohesion rising. The structural yield stress gradually increases with the amount of calcium oxide, and the stress-strain relationship also changes from strain hardening type to strain softening type.

4.4 NMR Analysis

The relaxation time T_2 spectrum (Fig. 6) reflects the pore content

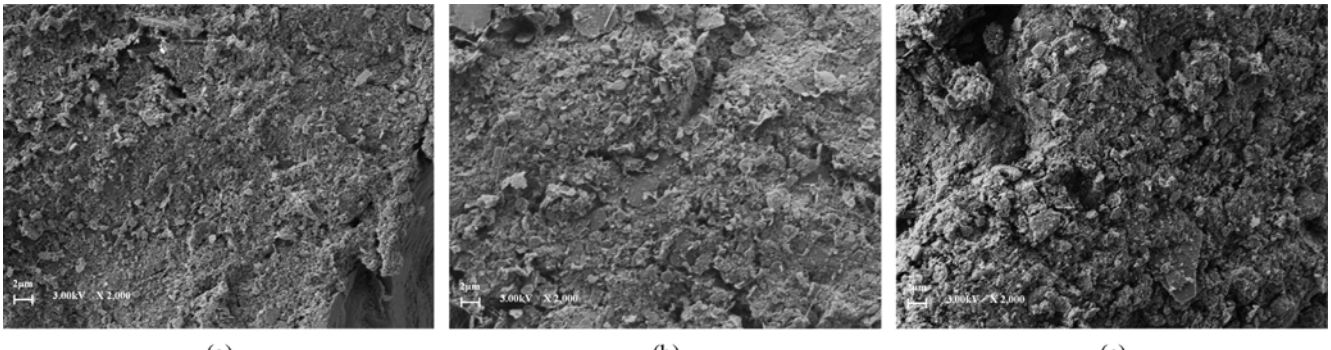

Fig. 5. SEM of Samples: (a) 0% Calcium Oxide Content, (b) 1% Calcium Oxide Content, (c) 8% Calcium Oxide Content

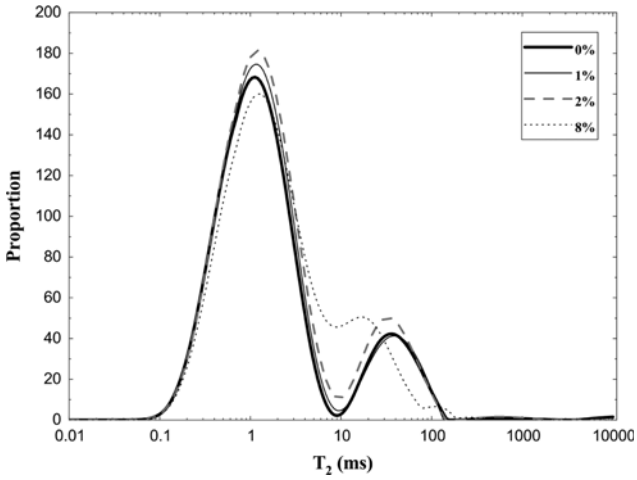

Fig. 6. T_2 Spectrum Curve with Different Calcium Oxide Content

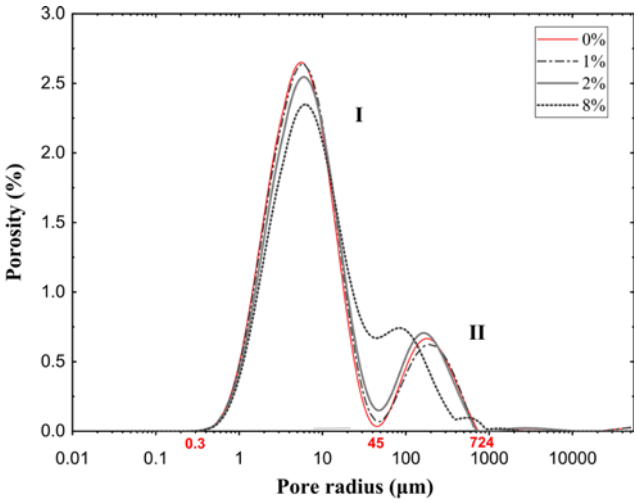

Fig. 7. Distribution of Pore Content in Red Clay Treated with Lime

and pore size distribution of lime-treated red clay. The graphic area enclosed by the curve of T_2 and the horizontal axis represents the pore content of the soil sample. The larger the area surrounded by the T_2 spectrum and the horizontal axis, the more the pore content in the soil sample. The red clay sample has an apparent bimodal distribution characteristic, a clear boundary between the peaks. It is indicating that the soil sample contains a large number of micropores and a small number of large pores. Even as the calcium oxide content increases, the boundary between the two peaks becomes more and more blurred, which indicates The addition of calcium oxide caused a change in the microstructure of the sample.

Table 3 shows the NMR signals of lime-treated red clay with different calcium oxide contents. Compared with untreated red clay, red clay mixed with calcium oxide has larger pores. As the calcium oxide content increases, the porosity first increases and then decreases. A small amount of calcium oxide makes the red clay alkaline and corrodes the red clay particles, causing pores to increase. As the content of calcium oxide increases, the hydration products produced with the red clay will cement the soil particles, thereby reducing the porosity. Alkaline corrosion of soil particles, calcium oxide, and red clay volcanic ash reaction, so that the agglomeration of soil can cause changes in pores. The results from the NMR test are consistent with the pore results observed by SEM.

The calculation of the aperture shows in Eq. (1):

$$T_2 = \frac{r_c}{\rho_2 F_s}, \tag{1}$$

where F_s is the pore shape influence factor (when spherical F_s = 3, when columnar F_s = 2); r_c is the radius of the pores. As can be seen, ρ_2 and F_2 are quantitative parameters. The relaxation time has a linear relationship with the pore radius. The size of the pores can be reflected by the relaxation time.

Table 3. Pore Signal of Lime-Treated Red Clay

Calcium oxide content (%)	0	1	2	8
Proportion	6346.283	6617.347	7119.563	6814.516
Porosity	6.57%	6.86%	7.41%	7.08%

The pore diameter of the soil calculated according to Eq. (1). In this study, the pores analyzed as spherical, so F_s = 2; according to the empirical method, take ρ_2 as 3 μm/ms (Liu et al., 2018).

Figure 7 shows the pore size distribution of the soil samples. The soil sample mainly consists of two peaks. The pores in the soil mainly consist of the first peak of 0.3 – 45 μm, the second peak of 45 – 724 μm, each peak spectrum is independent. 45 μm is the boundary between these two pores.

In the first peak in Fig. 7, the pore distribution interval of red clay with different calcium oxide content is similar. Still, the amplitude of the spectral lines decreases with the increase of the calcium oxide content. Which shows that the pore size of pore does not change significantly with calcium oxide, but the number of pores with a diameter of 0.3 – 45 μm decreases as the calcium oxide content increases. In the second peak in Fig. 7, it can be seen that the effect of calcium oxide on the pores between 45 and 724 μm is significant, and the impact on the pores around the pore diameter of 45 μm is particularly substantial. With the increase of the calcium oxide content, the number of pores with a pore size around 45 μm increases dramatically. The boundaries between the first peak and the second peak become more and more blurred, and the mesopores and small pores merge.

Lime will corrode the edges of kaolinite particles and produce CSH (Bell, 1996; Eisazadeh et al., 2012). Therefore, the number of pores with a size of 0.3 – 45 μm increases, which is mainly caused by calcium oxide eroding the edges of clay particles. Calcium oxide fills a large number of pores around 387 μm in diameter, which is due to soil flocculation caused by the exchange of clay minerals (Saba et al., 2014). The hydration reaction product produced by the volcanic ash reaction and calcium hydroxide fills the pores between 45 – 675 μm, resulting in changes in the pore structure.

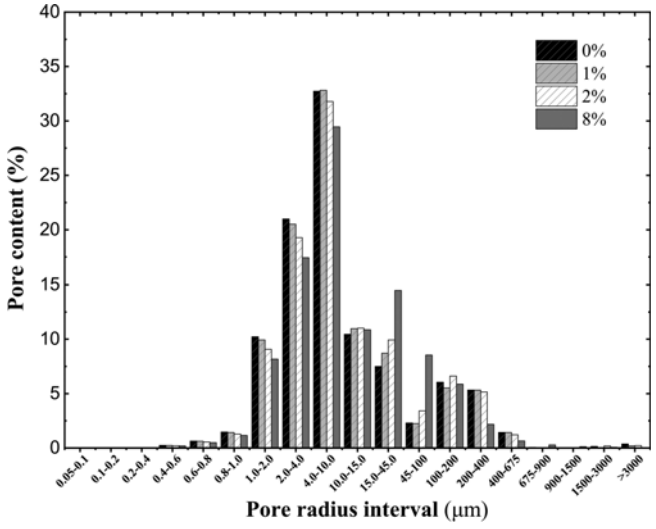

Fig. 8. Porosity Interval Distribution of Lime-Treated Red Clay

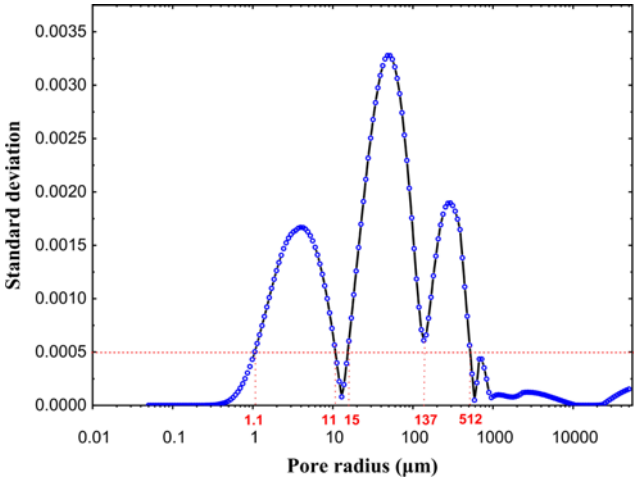

Fig. 9. The Standard Deviation of Pore Size of Lime-Treated Red Clay

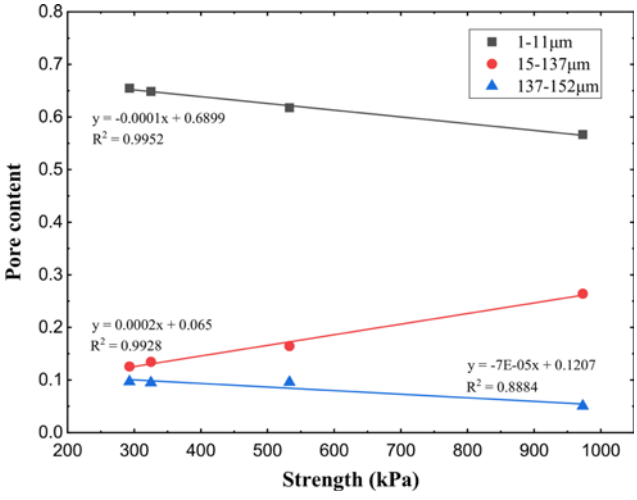

Fig. 10. The Relationship between Pore Content and Strength

The standard deviations of the pore sizes of 200 sizes with four calcium oxide contents (0%, 1%, 2%, and 8%) calculated. In probability statistics, standard deviation often used as a measure of statistical dispersion. It can reflect the dispersion among individuals in a group and is a measure of the dispersion of the average value of a group of data. A large standard deviation indicates a large difference between most values and their average; a small standard deviation means that these values are closer to the average (Fisher, 1919). The calculation of the standard deviation shown in Eq. (2):

$$S = \sqrt{\frac{\Sigma_{i=1}^{n}(X_i - \overline{X})^2}{n-1}}, \tag{2}$$

where S is the standard deviation, $\overline{X}$ refers to the arithmetic mean of the sample.

In order to analyze the effect of calcium oxide on the porosity of red clay, the standard deviation of the porosity of red clay under the calcium oxide content of 0%, 1%, 2%, and 8% was calculated. The standard deviation and pore distribution diagram are shown in Fig. 9. The standard deviation of some pore sizes is larger, which indicates that calcium oxide has a higher dispersion in the pore interval, which suggests that the change in the content of calcium oxide has a more significant effect in these pore sizes. In this study, pore diameters with a standard deviation higher than 0.0005 were selected for analysis. There are three intervals with a standard deviation of pore diameter higher than 0.0005. These are the interval I: 1.1 μm – 11 μm, II: 15 μm – 137 μm, and III: 137 μm – 512 μm. The largest standard deviation is the porosity of interval II, which indicates that the incorporation of calcium oxide has the greatest effect on the porosity of 15μm – 137μm in the sample.

Figure 10 is a scatter plot of the pore content and intensity of the three sections. From the scatter fitting line, the pore content of the three sections was linear with the peak values of the partial stress. Among them, the pore content in the pore interval I and III has a negative linear correlation with the strength. For lime-stabilized red clay, pores of 1.1 – 11 μm and 137 – 512 μm hurt soil strength. In the pore interval II, the porosity of 15 – 137 μm has a positive correlation with strength. The higher the pore content, the stronger the soil strength. This shows that the pores in this interval are conducive to soil strength. (Wang et al., 2012) found that under the condition of appropriate mass moisture content, moderate pinhole damage increased the triaxial shear strength of soil samples.

5. Conclusions

In the study, the triaxial compression test carried out on different amounts of calcium oxide treated red clay, and XRD analyzed the effect of calcium oxide on the chemical composition of red clay. Combined with the SEM and the low-field NMR, the impact of calcium oxide on the micropore structure of red clay was analyzed. Fit the content of the pores with the strength to obtain the linear relationship between them. The conclusions

drawn are as follows:

1. In the triaxial compression tests, calcium oxide has a significant effect on the strength of red clay. As the confining pressure increases, the impact of calcium oxide content on strength decreases significantly. It is because the mixing of calcium oxide with red clay produces hydration products that lead to an increase in cohesion.
2. Calcium oxide has a significant influence on the pore structure in the soil. The soil flocculation caused by the exchange of clay minerals and the formation of cement by volcanic ash reaction, which leads to the red clay changed from the granular and flaky to the agglomerate structure.
3. Low-field NMR showed that as the calcium oxide content increased, the porosity increased first and then decreased. It shows that the alkaline environment corrodes the soil particles and causes porosity to increase. The increased contain of calcium oxide will lead to the cementation material generated rising by the hydration reaction in the sample. That causes the particles in the soil to agglomerate and reduces the pores. "XRD indicated that calcium oxide chemically reacted to form calcium hydroxide. However, the curing time in this study was so short that the content of hydrated product was too low to be detected."
4. The pore evolution of red clay with different calcium oxide content calculate by variance, found that calcium oxide has the most significant influence on the pores of three intervals of red clay: I (1.1 – 11 μm), II (15 – 137 μm) and III (137 – 512 μm). The shear strength is linearly and negatively related to the pores in the I and III intervals, and positively associated with the pores in the II interval.

Acknowledgments

This study was supported by the National Natural Science Foundation of China (No. 41762022 and 41967037).

ORCID

Lijie Chen https://orcid.org/0000-0002-4134-7866
Xuejun Chen https://orcid.org/0000-0003-0679-3171
He Wang https://orcid.org/0000-0001-7229-6152
Xiang Huang https://orcid.org/0000-0003-3341-0826

References

Al-Mukhtar M, Belanteur N, Tessier D, Vanapalli S (1996) The fabric of a clay soil under controlled mechanical and hydraulic stress states. *Applied Clay Science* 11(2-4):99-115, DOI: 10.1016/S0169-1317(96)00023-3

Alonso E, Pinyol N, Gens A (2013) Compacted soil behaviour: Initial state, structure and constitutive modelling. *Géotechnique* 63(6):463-478, DOI: 10.1680/geot.11.P.134

ASTM D2850-15 (2013) Standard test method for unconsolidated-undrained triaxial compression test on cohesive soils. ASTM D2850-15, ASTM International, West Conshohocken, PA, USA

Bell FG (1996) Lime stabilization of clay minerals and soils. *Engineering Geology* 42(4):223-237, DOI: 10.1016/0013-7952(96) 00028-2

Bozbey I (2018) Microfabric evaluation of lime-treated clays by mercury intrusion porosimetry and environment scanning electron microscopy. *International Journal of Civil Engineering* 16(4B):443-456, DOI: 10.1007/s40999-017-0151-5

Changizi F, Haddad A (2017) Effect of nanocomposite on the strength parameters of soil. *KSCE Journal of Civil Engineering* 21(3):676-686, DOI: 10.1007/s12205-016-1471-8

Chen L, Chen, Yang X, Bi P, Ding X, Huang X, Wang H (2020) Effect of calcium carbonate on the mechanical properties and microstructure of red clay. *Advances in Materials Science and Engineering* 2020, DOI: 10.1155/2020/5298186

Daigle H, Johnson A (2016) Combining mercury intrusion and nuclear magnetic resonance measurements using percolation theory. *Transport in Porous Media* 111(3):669-679, DOI: 10.1007/s11242-015-0619-1

Delage P, Lefebvre G (1984) Study of the structure of a sensitive Champlain clay and of its evolution during consolidation. *Canadian Geotechnical Journal* 21(1):21-35, DOI: 10.1139/t84-003

Eisazadeh A, Kassim K, Nur H (2012) Stabilization of tropical kaolin soil with phosphoric acid and lime. *Natural Hazards Journal* 61(3):931-942, DOI: 10.1007/s11069-011-9941-2

Eltwati A, Tarhuni F, Elkaseh A (2020) Engineering properties of clayey soil stabilized with waste granite dust. *Journal of Critical Reviews* 7(16):794-802

Fisher RA (1919) XV. The correlation between relatives on the supposition of mendelian inheritance. *Transactions of the Royal Society of Edinburgh* 52(2):399-433, DOI: 10.1017/S0080456800012163

Fleury M, Berthe G, Chevalier T (2019) Diffusion of water in industrial cement and concrete. *Magnetic Resonance Imaging* 56:32-36, DOI: 10.1016/j.mri.2018.09.010

Gallegos DP, Smith DM (1988) A NMR technique for the analysis of pore structure: Determination of continuous pore size distributions. *Journal of Colloid and Interface Science* 122(1):143-153, DOI: 10.1016/0021-9797(88)90297-4

GB/T 50123-1999 (1999) National standard of the People's Republic of China. Standard for geotechnical testing method. GB/T 50123-1999, CSBTS & Ministry of Construction, Beijing, China

Ghobadi MH, Abdilor Y, Babazadeh R (2014) Stabilization of clay soils using lime and effect of pH variations on shear strength parameters. *Bulletin of Engineering Geology and the Environment* 73(2):611-619, DOI: 10.1007/s10064-013-0563-7

Guidobaldi G, Cambi C, Cecconi M, Comodi P, Deneele D, Paris M, Russo G, Vitale E, Zucchini A (2018) Chemo-mineralogical evolution and microstructural modifications of a lime treated pyroclastic soil. *Engineering Geology* 245:333-343, DOI: 10.1016/j.enggeo.2018.09.012

Jaeger F, Bowe S, van As H, Schaumann G (2009) Evaluation of 1H NMR relaxometry for the assessment of pore-size distribution in soil samples. *European Journal of Soil Science* 60(6):1052-1064, DOI: 10.1111/j.1365-2389.2009.01192.x

Kilic R, Kucukali O, Ulamis K (2016) Stabilization of high plasticity clay with lime and gypsum (Ankara, Turkey). *Bulletin of Engineering Geology and the Environment* 75(2):735-744, DOI: 10.1007/s10064-015-0757-2

Koliji A, Vulliet L, Laloui L (2010) Structural characterization of unsaturated aggregated soil. *Canadian Geotechnical Journal* 47(3):297-311, DOI: 10.1139/T09-089

Lemaire K, Deneele D, Bonnet S, Legret M (2013) Effects of lime and cement treatment on the physicochemical, microstructural and

mechanical characteristics of a plastic silt. *Engineering Geology* 166:255-261, DOI: 10.1016/j.enggeo.2013.09.012

Liang C, Xiao LZ, Zhou CC, Zhang Y, Liao GZ, Jia ZJ (2019) Two-dimensional nuclear magnetic resonance method for wettability determination of tight sand. *Magnetic Resonance Imaging* 56:144-150, DOI: 10.1016/j.mri.2018.09.020

Lin BT, Cerato AB (2015) Shear strength of shale weathered expansive soils along swell-shrink paths: Analysis based on microscopic properties. *Environmental Earth Sciences* 74(9):6887-6899, DOI: 10.1007/s12665-015-4691-1

Liu Y, Li Z, Guo L, Kang W, Zhou Y (2018) Pore characteristics of soft soil under triaxial shearing measured with NMR. *Chinese Journal of Rock Mechanics and Engineering* 37(08):1924-1932, DOI: 10.13722/j.cnki.jrme.2018.0118 (in Chinese)

Lv Q, Chang C, Zhao B, Ma B (2018) Loess soil stabilization by means of SiO_2 nanoparticles. *Soil Mechanics and Foundation Engineering* 54(6):409-413, DOI: 10.1007/s11204-018-9488-2

Oualmakran M, Mercatoris B, Francois B (2016) Pore-size distribution of a compacted silty soil after compaction, saturation, and loading. *Canadian Geotechnical Journal* 53(12):1902-1909, DOI: 10.1139/cgj-2016-0184

Saba S, Delage P, Lenoir N, Cui YJ, Tang AM, Bamichon JD (2014) Further insight into the microstructure of compacted bentonite-sand mixture. *Engineering Geology* 168:141-148, DOI: 10.1016/j.enggeo.2013.11.007

Saeed KA, Kassim KA, Nur H (2015) Strength of lime-cement stabilized tropical lateritic clay contaminated by heavy metals. *KSCE Journal of Civil Engineering* 19(5):887-892, DOI: 10.1007/s12205-013-0086-6

Sakr MA, Shahin MA, Metwally YM (2008) Utilization of lime for stabilizing soft clay soil of high organic content. *Geotechnical and Geological Engineering* 27(1):105, DOI: 10.1007/s10706-008-9215-2

Shan Y, Mo H, Yu S, Chen J (2016) Analysis of the maximum dynamic shear modulus and particle arrangement properties of saturated soft clay soils. *Soil Mechanics and Foundation Engineering* 53(4):226-232, DOI: 10.1007/s11204-016-9390-8

Tchalenko J, Morgenstern N (1967) Microscopic structures in kaolin subjected to direct shear. *Géotechnique* 17(4):309-328, DOI: 10.1680/geot.1967.17.4.309

Tovey N (1980) A digital computer technique for orientation analysis of micrographs of soil fabric. *Journal of Microscopy* 120(3):303-315, DOI: 10.1111/j.1365-2818.1980.tb04150.x

Wang S, Chen Z, Li X, Peng Z, Yuan J (2012) Pore-damage evolution and mechanical properties of remolded soil by CT-triaxial test. *Transactions of the Chinese Society of Agricultural Engineering* 28(07):150-154, DOI: 10.3969/j.issn.1002-6819.2012.07.025 (in Chinese)

Wang J, Xiao LZ, Liao GZ, Zhang Y, Cui YS, Sun Z, Dong Y, Hu L (2019) NMR characterizing mixed wettability under intermediate-wet condition. *Magnetic Resonance Imaging* 56:156-160, DOI: 10.1016/j.mri.2018.09.023

Yunus NZM, Wanatowski D, Hassan NA (2016) Shear strength and compressibility behaviour of lime-treated organic clay. *KSCE Journal of Civil Engineering* 20(7):1721-1727, DOI: 10.1007/s12205-015-0438-5

Zhao H, Ge L, Petry T, Sun Y (2014) Effects of chemical stabilizers on an expansive clay. *KSCE Journal of Civil Engineering* 18(5):1009-1017, DOI: 10.1007/s12205-013-1014-5

Zimmermann I, Filser S, Mordhorst A, Fleige H, Horn R (2019) Structural stabilization of soil backfill with quicklime. *Journal of Plant Nutrition and Soil Science* 182(4):578-585, DOI: 10.1002/jpln.201800511